ISSN: 2278-4632
Vol-10 Issue-2 No.01 February 2020

MgB4O7:Ce, Li-based films: feasibility investigations for 2D optically stimulated luminescence dosimetry

Amit Kumar Jana[1], Rojalin Sadual[2]
[1,2] Gandhi Institute for Education and Technology, Baniatangi, Bhubaneswar

A B S T R A C T

The aim of this study is to identify existing limits of this material for this application and to establish the possibility of 2D dosimetry utilizing optically stimulated luminescent (OSL) films based on MgB4O7:Ce,Li. After irradiation, a small batch of test films was created and scanned with a laser-scanning OSL scanner. Additionally, the dosimetric characteristics and luminescence of OSL were examined. The findings highlight the benefit of the short luminescence lifespan (~31.5 ns) linked to Ce3+ emission for 2D dosimetry utilizing laser-scanning reading, as it reduces the requirement for pixel-bleeding correction. An appropriate bleaching of the signal might be achieved with a long-pass filter and a fluorescent bulb. Pieces of film representing steep dose gradients could be used to create a dose response curve, and the dose response derived utilizing the signal from the center of such piece films was linear up to 10 Gy. The lumines- cence signal of MgB4O7:Ce,Li has both short- and long-term phosphorescence components, although their contribution to the fast OSL signal is negligible and should diminish as laser scan speeds increase. The primary drawback of MgB4O7:Ce,Li at the time is the absence of a deeper comprehension of the mechanisms accountable for the sensitivity variations and fading of the OSL signal, despite the material's high OSL sensitivity and linear response. Despite the bleaching used here being able to bring the remaining OSL signal down to negligible levels (<1 mGy), the films' sensitivity rose with the prior dosage. It has also been shown that fading has a greater impact on the initial OSL intensity than the OSL area. This study also emphasizes the necessity of delving deeper into the luminescence processes of MgB4O7:Ce,Li in order to have a better understanding.

1. Introduction

In modern radiation therapy, increasingly complex dose distributions can be created to improve the treatment. Nevertheless, the convenient acquisition of high-precision and accurate 2D dosimetry data with high spatial resolution to verify such dose distributions is to date still not a reality in practice, as can be seen from a discussion on available techniques [1,2].

Furthermore, new challenges arising from the need to measure dose distributions at very high dose rates (>100 Gy/s) as proposed in FLASH radiotherapy [3–6] or in the presence of magnetic fields in magnetic-resonance-guided radiotherapy (MRgRT) [7–11] makes the development of techniques that can cope with these extreme conditions even more urgent. Radiochromic films [12] and ionization chamber or diode arrays [13–15] have intrinsic limitations.

Radiochromic films are not re-usable and have a very limited dynamic range due to the intrinsic signal of the un-irradiated films on the low dose range (typically equivalent to > 100 mGy), and signal saturation at the high-dose range; for examples of dose response curves, see Refs. [16–18].

Dosimetry using radio- chromic films also requires a triple-channel algorithm to eliminate the effect of film non-uniformities, which in turn requires calibration of the three channels for each film batch [18]. Ionization chamber or diode arrays provide only sparse dose information (>mm spacing) and include non-tissue equivalent components [19,20].

The above techniques are also problematic in the case of high dose rates or in the presence of magnetic fields [21–23]Because of the above limitations, several groups have attempted to take advantage of the intrinsic properties of optically stimulated luminescence (OSL), a technique widely used in dosimetry and for imaging in computed radiography for 2D dosimetry [24–29]. In addition to providing a wide linear dynamic range and intrinsically no background (zero dose) signal, OSL also allows the development of re-usable films [29].

At the moment, no data on the effect of extreme dose rates on OSL detectors is available. Nevertheless, because the techniques is based on solid-state detection, it is expected to show little to no dose-rate dependence and is, therefore, of interest for dosimetry in FLASH radiotherapy. OSL relies on radiation-induced trapped charges in inorganic crystalline insulators, which can be read out in laboratory by stimulation with light; see Bøtter-Jensen et al. [30], Yukihara and McKeever [31] or Kry et al. [32] for more details on the technique.

Because the OSL signal is usually measured at shorter wavelengths than the stimulation light, the OSL measurements have low background, showing no intrinsic signal when not irradiated [30]. This means that the ubiquitous Stokes-shifted luminescence observed from plastic, dust, and other photoluminescence processes within the crystal are not detected and the background is typically only instrumental, due to dark counts in the photomultiplier tube (PMT) or leakage of stimulation light into the detection system.

This is in strong contrast with other techniques such as radiochromic films, which have inherently a high intrinsic background even without expo- sure [20]. Furthermore, the OSL signals are linear from the minimum doses that can be detected up to tens or hundreds of grays. OSLDs have also been shown to be essentially independent of the magnetic field [33] and, up to now, no dependence on dose rate has been reported. OSL has already been used for imaging in computed radiography (CR), but the material used in CR is not suitable for dosimetry because of the high effective atomic number (Zeff of BaFBr = 56 and Zeff of CsBr is 49) [34,35].

The use of such films for 2D dosimetry is generally prob- lematic because of the strong photon energy dependence in the energy range below 300 keV.

Fading of such materials also need mitigation [29, 36–39]. New phosphors have been attempted, but also with similar problems (e.g. SrS:Ce,Sm, KCl:Eu^{2+}, $NaMgF_3$:Eu^{2+}) [28,40,41]. To avoid the pitfalls above, we previously focused on a widely used dosimetric material, Al_2O_3:C, and its

ISSN: 2278-4632
Vol-10 Issue-2 No.01 February 2020

related compound, Al_2O_3:C,Mg, for 2D dosimetry.

Films containing either Al_2O_3:C or Al_2O_3:C,Mg were pro- duced by Landauer Inc. and a laser-scanning system was built to carry out feasibility tests and identify the main limitation of using such materials for 2D dosimetry [42].

An algorithm was developed to circumvent the main disadvantage of Al_2O_3 for laser-scanning readout, which is the long luminescence lifetime (35 ms) of the main luminescence centers, F-cen- ters [43], and to implement other needed corrections [44].

The performance of the algorithm is aided by the presence of a fast luminescence centers, F+-centers (lifetime < 6 ns), particularly in Al2O3:C,Mg, allowing the use of scan speeds orders of magnitude faster than what would be possible due to the 35 ms lifetime of the F-centers.

The pixel dwell time (time the laser spends in each pixel) used was 326 μs, in comparison with the ~100 ms that would be required if the pixel dwell time were three times the luminescence lifetime, which is recommended to avoid pixel bleeding [45].

The system was tested using a 6-MeV clinical photon beam [24] and showed linearity from the minimum detectable dose (<1 mGy) up to > 1 Gy followed by a supralinear behavior, but no saturation up to >70 Gy.

The system was also demonstrated for ion beam therapy [46]. In spite of the results above, laser-scanning readout of Al_2O_3:C pre- sents still some limitations.

The spectral overlap between the fast F^+- center emission and the slow F-center emission has so far prevented isolation of the fast luminescence center exclusively by using optical filters, which would mitigate the pixel-bleeding problem.

Furthermore, the luminescence from F^+-center is relatively weak in comparison with the F-center emission, even in Al_2O_3:C,Mg materials, and its luminescence (broadband centered at 330 nm) is not well transmitted by plastic light guides. The proposed pixel-bleeding correction algorithm also introduces additional noise to the data.

For the above reasons, we tried to identify and develop new materials with the proper combination of host and dopant to achieve the appropriate dosimetric properties and fast luminescence for laser scanning. The best candidate identified so far is MgB_4O_7:Ce,Li, a matrix with low effective atomic number (Z_{eff} = 8.4). The material present OSL intensity comparable to Al_2O_3:C.

The dominant TL peak is situated at ~210 °C (at 1 °C/s) and is associated with the OSL signal. The dose response is linear up to ~10 Gy and saturation only occurs above ~1000 Gy [47]. The OSL emission is from Ce^{3+}, with a lifetime of 31.5 ns [48]. The material has also been produced by other groups using solid state reaction and was identified as a promising material for OSL dosimetry [49].

In spite of its interesting properties of MgB4O7:Ce,Li for 2D dosimetry, there are still two phenomena that affect the performance of MgB4O7:- Ce,Li: sensitization and fading.

Sensitization refers to the increase in sensitivity with repeated use and fading is the decrease in signal at room temperature. The mechanism behind these phenomena is complex and still under investigation [47,48]. Nevertheless, it is important to deter- mine the degree of sensitization and fading under the current conditions.

The objective of this work is to demonstrate the feasibility of 2D dosimetry using films containing MgB_4O_7:Ce,Li and to identify current limitations. A small quantity of test films were produced by Agfa NV (Mortsel, Belgium) using MgB_4O_7:Ce,Li produced at Oklahoma State University (Stillwater, Oklahoma, USA).

We investigated the performance of the films using laser-scanning readout and the luminescence and dosimetric properties that affect its performance. This works focuses exclusively on the luminescence properties; a complete demonstration of the clinical application is outside the scope of this work, as it would require the production of a larger quantity of films and further optimization of material and of the film casting process. Nevertheless, we hope that the results presented here will motivate further developments in this direction.

2. Materials and methods

2.1. Samples

MgB_4O_7:Ce,Li powder was prepared as previously described using high purity reagents and a nominal concentration in the starting solution of 0.3 mol% Ce and 10 mol% Li [48].

Examples of the film and samples cut from the films are shown in Fig. 1. To prepare the films, 21.50 g of a 20% Kraton™ FG1901X solution (Kraton Co.) in toluene and 0.40 g of a Baysilone® (low molecular weight methyl polysiloxane; OMG Borschers GmbH) solution in toluene were added to 16.3 g of toluene. 2.7 g of MgB_4O_7 phosphor and 9.1 g of Lanco™ Wax TF1780 (The Lubrizol Co.) were dispersed in the obtained binder solution. The dispersion was homogenized for 5 min using an Ultra Turrax mixer (IKA®-Werke GmbH & Co., Staufen, Germany)

Fig. 1. Film samples produced by Agfa NV using MgB_4O_7:Ce,Li synthesized at Oklahoma State University, as well as additional samples prepared for the investigations described here.

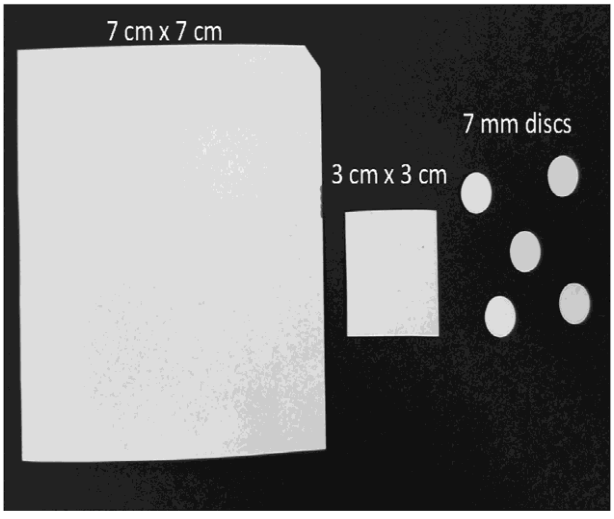

ISSN: 2278-4632
Vol-10 Issue-2 No.01 February 2020

operated at 9600 rpm. The homogenized lacquer was filtered over a filter cloth with a mesh size of 75 µm. The obtained lacquer was coated on a 175 µm clear PET substrate by doctor-blade coating. Wet thickness was 550 µm. The coated layer was left to dry at room temperature.

Al_2O_3:C and Al_2O_3:C,Mg films described in Ahmed et al. [46] were also used for comparison.

2.2. *Characterization equipment*

2.2.1. *2D OSL reader*

The laser-scanning system used for imaging the OSL films was described by Ahmed et al. [42] and later updated [44]. The system consists of a 532 nm DPSS laser (model GMLN-532-100FED, 100 mW output power, Lasermate Group, Inc.) for stimulation. A 2D galvanometer mirror system (model GVS002, Thorlabs, Inc.) is used to reflect and scan the laser to the OSL film placed on top of a Schott GG-495 long-pass filter (15.0 cm × 15.0 cm × 3.5 mm, Schott Glass Corporation). A Hoya U-340 band-pass filter (15.0 cm × 15.0 cm × 3.0 mm thick, Hoya Corporation) is placed on top of the film to keep the films flat. An additional 5.0-mm thick Hoya U-340 filter is placed in front of the PMT (PMT; 51 mm diameter, 9235QA, Electron Tubes Inc.) to block any laser light reaching the PMT. The signal recorded by the PMT is amplified by a pre-amplifier (model SR-445, Stanford Research Systems) and digitized using a multichannel scaler (model SR-430, Stanford Research). During a readout, consecutive rows of the film are scanned in opposite directions separated by ~0.17 mm (~13.0 cm total scan length, 751 bins). Each scanned row is divided into 1024 bins with each bin equivalent to 327.68 µs (bin width) and ~0.13 mm (~13.0 cm total scan length, 1024 bins). Because the laser scan is performed based on angle variation of the two galvo mirrors, the raw images do not correspond to linear dimensions. Geometrical distortion correction is required to transform the images to true linear dimensions; see Ahmed et al. [44] for more details. The laser power is constantly monitored with a photodiode during scanning (model DET10A, Thorlabs, Inc.).

2.2.2. *Risoe readers*

Luminescence characterization of the detectors were performed using two Risø TL/OSL readers (DTU Nutech, Denmark). The Risø reader model TL/OSL-DA-15 at Oklahoma State University is equipped with a 1.48 GBq $^{90}Sr/^{90}Y$ beta source delivering a dose rate of ~69.5 mGy/s to the sample position. The emitted light from the sample was detected using a photomultiplier tube (PMT, model 9235QA, Electron Tubes) using Hoya U- 340 filters (7.5 mm thickness, Hoya Corporation) in front of the PMT. Blue (broad band centered at 470 nm, ~30 mW/cm^2) or green LEDs (broad band centered at 525 nm, ~10 mW/cm^2) were used for stimulation.

Further measurements were performed using a Risø reader model TL/ OSL-DA-20 at the Paul Scherrer Institute, which is equipped with ac- cessories for lifetime measurements. This reader is equipped with a 1.48 GBq $^{90}Sr/^{90}Sr$, but the dose rate is ~35 mGy/s because of a larger source- to-sample distance. The samples were stimulated with blue LEDs (broad band centered at 470 nm, irradiance of 81 mW/cm^2 at the sample posi- tion) and the light was detected using an ET Enterprises PMD9107Q-AP- TTL photomultiplier tube (PMT). Hoya U-340 filters (Hoya Corporation, 7.5 mm thickness) were used in front of the PMT. The reader is equipped with a software-controlled Detection and Stimulation Head (DASH) [50]. The Risø TL/OSL-DA-20 reader is also equipped with a Photon Timer attachment (Time-Correlated Single Photon Counter board, PicoQuant TimeHarp 260) for lifetime and time-resolved measurements [51]. The samples were stimulated with 150 µs blue LED pulses every 200 ms for 2000 s. Each photon is time-tagged and the photon arrival time can be plotted for various bin widths to analyze the luminescence signal during and after the LED pulses.

2.2.3. *Bleaching unit*

The OSL bleaching unit consists of two halogen lamps, the lamp output being filtered using Schott GG-400 long-pass filter (3.0 mm thick, Schott Corporation). The average irradiance at the sample position was ~2.4 mW/cm^2.

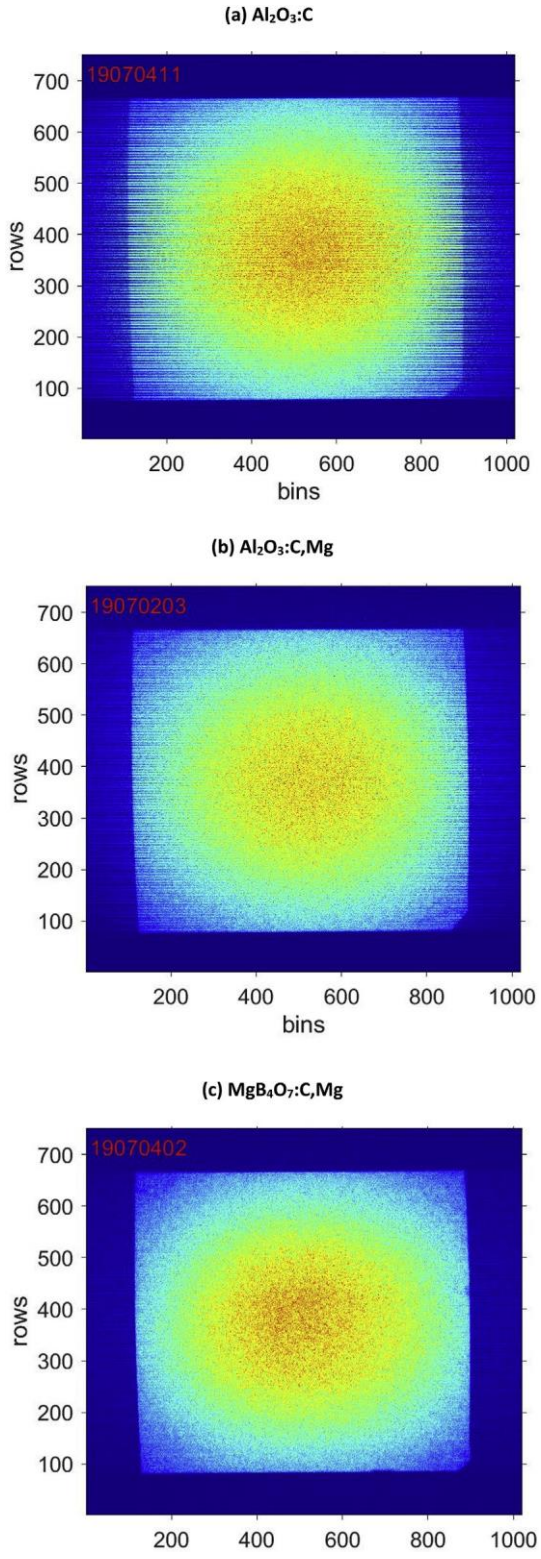

Fig. 2. Raw OSL images from 10.0 cm × 10.0 cm OSL films of (a) Al_2O_3:C, (b) Al_2O_3:C,Mg, and (c) MgB_4O_7:Ce,Li irradiated using the 90 kVp x-ray source in air with ~0.76 Gy total dose. The image is approximately 13.0 cm × 13.0 cm and the pixels are separated by ~0.13 mm in the scan (x-axis) direction and ~0.17 mm in the sub-scan (y-axis) direction (see Section 2.4).

ISSN: 2278-4632
Vol-10 Issue-2 No.01 February 2020

2.3. Irradiations

In addition to the $^{90}Sr/^{90}Y$ sources in the Risø readers (Section 2.2.2), film irradiations were carried out using a 90 kVp cabinet X-ray system (10–110 kV output voltage, 3 mA continuous current, Faxitron 43805 N, Hewlett- Packard, air kerma rate of ~38 mGy/min, ~46 cm source-to- sample distance) because of the larger irradiation area. Irradiations of small detectors were also carried out using a stand-alone 100 mCi $^{90}Sr/^{90}Y$ beta irradiator (~1 mGy/s, ~10 cm source-to-sample distance) because of the more uniform dose rate.

2.4. Data analysis

The image reconstruction algorithm was identical to the one described by Ahmed et al. [44], except that in the case of MgB_4O_7:Ce,Li the lifetimes of the slow components (slow luminescence centers or phosphorescence) and relative ratio between fast and slow luminescence centers used in the pixel-bleeding algorithm [43] were adjusted. Because of the geometrical distortion introduced by the galvo mirrors setup, the data points are not equally spaced in the film plane and, therefore, the bin position in the raw images cannot be converted into linear dimensions (e.g. cm) by a simple factor, requiring a complex model of the imaging system [44]. After correction for the geometrical distortion to obtain the linear dimensions, the data points are averaged within 0.25 mm x 0.25 mm pixels (~100 dpi) to obtain points equally spaced in the film plane and facilitate further analysis.

3. Results and discussion

3.1. Comparison of raw images

OSL films (10.0 cm × 10.0 cm) based on carbon-doped aluminum oxide (Al_2O_3:C), aluminum oxide doped with carbon and magnesium (Al_2O_3:C,Mg) and magnesium borate (MgB_4O_7:Ce,Li) were irradiated in air using the 90 kVp X-ray source with an air kerma of ~ 0.76 Gy and read using the 2D OSL system (see Section 2.2.1) in the same readout condi- tions, with fast scanning in alternate horizontal directions with a pixel dwell time of 327 μs bin^{-1}.

Fig. 2 compares the raw (uncorrected) images of an MgB_4O_7:Ce,Li film with those of Al_2O_3:C and Al_2O_3:C,Mg films. Since the scanning area is larger than the film size, the different influence of pixel bleeding can be observed particularly at the edges of the film in the fast-scan direction (horizontal). Whereas pixel bleeding due to the slow luminescence life- time of F-center (~ 35 ms) is evident in the Al_2O_3:C (Fig. 2a) and Al_2O_3:C,Mg images (Fig. 2b), the MgB_4O_7:Ce,Li image (Fig. 2c) shows essentially no pixel bleeding. Al_2O_3:C,Mg films show less pixel bleeding than the Al_2O_3:C films because of the larger relative concentration of fast F^+-centers, but pixel bleeding correction is still necessary because of the difficulty to completely separate the F and F^+-center emission bands in Al_2O_3.

In these raw images the signal at the center is more intense and the film shape outline is distorted because the images were not yet corrected for the light collection efficiency and geometrical distortion of the system [44].

The relative amount of pixel bleeding can be better visualized in the normalized profiles shown in Fig. 3, calculated from the raw images from Fig. 2 using only scans in the positive direction. The figure shows the scans (average of 10 rows) in the fast-scan directions (horizontal or x- direction).

Both Al_2O_3 films show a distorted profile and a tail of luminescence after the film ends (~pixel 900) due to pixel bleeding. The MgB_4O_7:Ce,Li film shows both a fast rise at the beginning of the scan (~pixel 110) and a sharp drop at the end of the scan (~pixel 900), thus demonstrating the improved imaging provided by the fast Ce^{3+} emission centers.

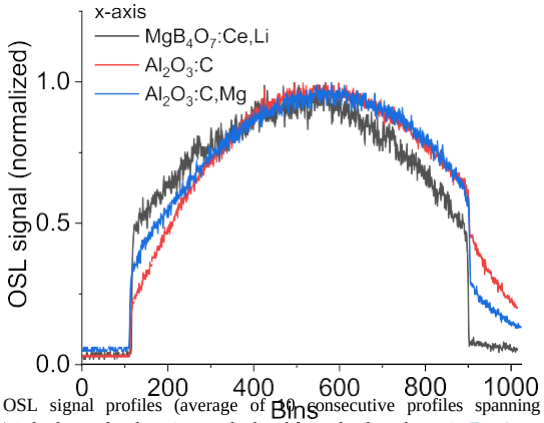

Fig. 3. OSL signal profiles (average of 10 consecutive profiles spanning ~2.0 mm) in both x and y-directions, calculated from the data shown in Fig. 2.

The OSL from the MgB_4O_7:Ce,Li film in Fig. 3 is less intense, but this is partly due to its lower effective atomic number (Z_{eff} = 8.4) in comparison to Al_2O_3 (Z_{eff} = 11.3), which leads to a lower energy absorption upon X- ray exposure.

3.2. Basic luminescence properties of MgB_4O_7:Ce,Li

3.2.1. OSL signal depletion per readout

The OSL signal depletion per readout is important because it de- termines the OSL signal read during each scan and the signal remaining for re-evaluation of the film. By controlling the laser intensity, one can increase how much signal is read per scan, but this consequently de- creases how much signal is left for re-evaluation (if needed).

Therefore, the OSL depletion per readout was compared in the cur- rent experimental conditions (laser power, wavelength and scan speed) for the three different films (MgB_4O_7:Ce,Li, Al_2O_3:C and Al_2O_3:C,Mg films) by irradiating them in air using the 90 kVp x-ray source with a total dose of ~ 0.76 Gy and then reading them nine times in sequence using the 2D OSL system. The images were then corrected using the image reconstruction algorithm (Section 3.3).

Fig. 4 compares the OSL signal in a 1.0 cm × 1.0 cm region of interest (ROI) as a function of the readout number. In the current experimental conditions, only ~25–30% of the OSL signal is read per scan for all three film types. If the signal intensity is sufficient for 2D dosimetry, this means that the films can be repeatedly scanned to re-measure the dose profiles in the future, provided a correction for depletion is applied. Repeated scans can also be performed for improved statistics.

Nevertheless, the data also shows that the MgB_4O_7:Ce,Li films are bleached more slowly than the Al_2O_3 films. Shorter wavelengths or higher stimulation intensities can be used to increase the amount of signal per scan. Blue light is more appropriate to stimulated the OSL in MgB_4O_7:Ce,Li [48] than the green light used here. In the case of Al_2O_3:C, green light is preferable, as blue stimulation leads to unwanted photo-transfer effects [52].

3.2.2. Luminescence lifetime components

Time-Correlated Single Photon Counting (TCSPC) (Section 2.2.2) measurements of MgB_4O_7:Ce,Li, Al_2O_3:C and Al_2O_3:C,Mg films irradiated with ~2.1 Gy were performed to compare the relative contribution of fast and slow luminescence components in the different samples. The lumi- nescence was measured for a total of 1000 s using 150 μs blue LED pulses every 200 ms (a total of 5000 pulses). The data were analyzed using the PTanalyse software (DTU Nutech, Risø Campus, Denmark) with 512 ns bin width to observed the fast luminescence component and with 32.8 μs to observe the slow luminescence component.

ISSN: 2278-4632
Vol-10 Issue-2 No.01 February 2020

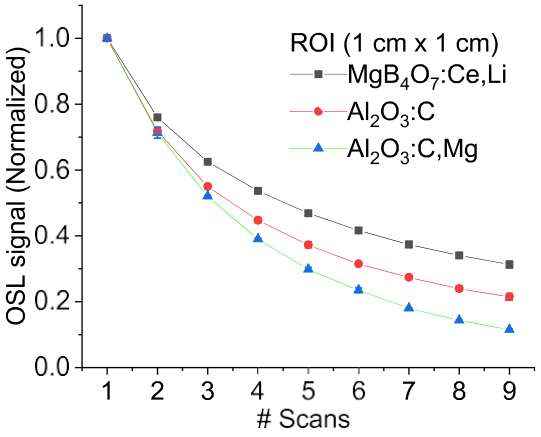

Fig. 4. Signal depletion normalized to the center of image (ROI 1.0 cm × 1.0 cm) from first scan of MgB_4O_7:Ce,Li, Al_2O_3:C and Al_2O_3:C,Mg. Each data point is average of three sets of measurements. The error bars represent the standard deviation between the three measurements. The depletion was then fitted with a double exponential. The samples were read using 100% laser power.

Fig. 5 shows data for the fast (Fig. 5a) and slow luminescence com- ponents (Fig. 5b). During the LED pulse, all three samples show a fast response due to the fast luminescence centers (Ce^{3+} in the case of MgB_4O_7:Ce,Li and F^+-centers in the case of Al_2O_3) (Fig. 5a). After the LED pulse, Al_2O_3:C is characterized by a clear 35 ms decay component asso- ciated with the F-centers (Fig. 5b). Al_2O_3:C,Mg is characterized by an additional (2.4 ms) component due to trapping centers below room temperature as well as a higher vertical offset due to long lifetime com- ponents associated with shallow traps above room temperature [53]. MgB_4O_7:Ce,Li shows some small short lifetime component immediately after the LED pulse (Fig. 5a) likely due to shallow traps below room temperature, lower luminescence in an intermediary timescale (~0.5–100 ms) and a larger offset than Al_2O_3:C likely due to shallow traps above room temperature. In the case of MgB_4O_7:Ce,Li, ~54% of the light was emitted during the 150 μs LED pulse, whereas in the case of Al_2O_3:C and Al_2O_3:C,Mg only 17% and 22% of the light is emitted during the LED pulse. The results of the fittings are presented in Table 1.

This demonstrates that MgB_4O_7:Ce,Li is a more appropriate material for laser scanning applications from the point of the view of the lumi- nescence lifetime, although some slower components likely associated with shallow traps below room temperature may have to be corrected for. The lifetime components of MgB_4O_7:Ce,Li films could not be unambig- uously determined; depending on the timescale of the acquisition, a different value for the lifetime is obtained. This may be an indication that the luminescence does not have one dominant component. That would be the case if the slow luminescence components associated to shallow trapping centers with a broad activation energy distribution. In this case, the lifetime needs to be determined for the specific parameters used in the film readout.

3.2.3. *Phosphorescence signal*

To characterize the phosphorescence components, five sets each with three 7.0-mm diameter MgB_4O_7:Ce,Li samples were irradiated with different doses and read out immediately after irradiation using the Risø TL/OSL-DA-15 reader. The phosphorescence signal was measured for an hour after each sample's irradiation.

Fig. 6 presents the phosphorescence intensity after irradiation, normalized to the initial OSL intensity during readout. The error bars indicate the standard deviation between the three samples used for each dose. Immediately after irradiation, the phosphorescence signal is ~10% of the OSL signal for the samples irradiated with 0.069 Gy dose, but it decreased to <1% within 15 min after irradiation for all the doses

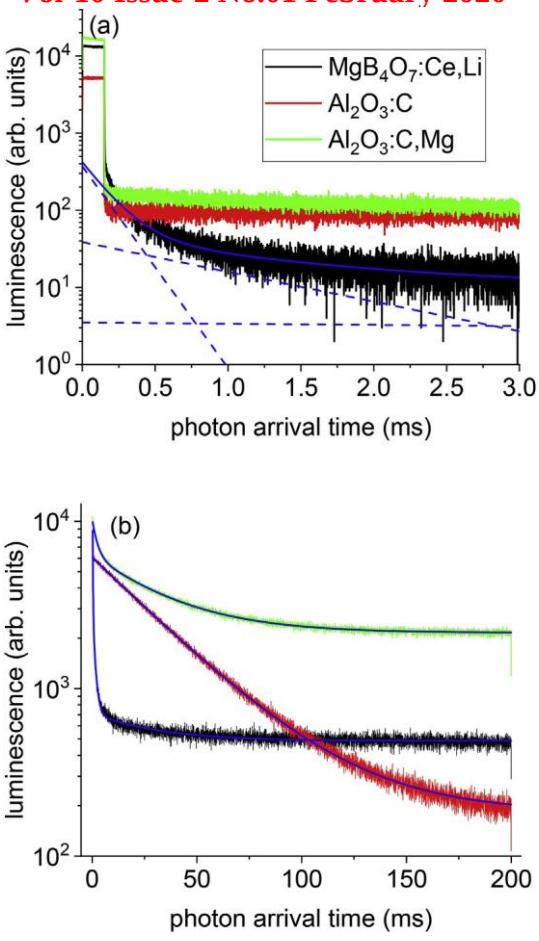

Fig. 5. OSL signal of Al_2O_3 and MgB_4O_7:Ce,Li films to a 1.0 μs LED pulse as a function of both photo arrival time and stimulation time measured using Time- Correlated Single Photon Counting (TCSPC), represented in two timescales: (a) up to 3.0 ms and (b) up to 200 ms. The dashed curves in (a) shows the com- ponents of the MgB_4O_7:Ce,Li fit and (b) shows only the total fits.

Table 1
Parameters obtained from fitting the photon arrival time curves in Fig. 5b.

Parameters	MgB_4O_7:Ce,Li	Al_2O_3:C	Al_2O_3:C,Mg
a	(243 4)×10¹	5910 3	(402 2)×10¹
b	(238 3)×10²	*	4105 9
c	224 3	*	*
t1	1.24 0.01	35.09 0.03	2.38 0.02
t2	0.166 0.002	*	33.07 0.10
t3	29.27 0.06	*	*
y0	487.4 0.6	183.5 1.0	2155.8 1.7

delivered.

The results indicate that a 15 min wait between irradiation and readout should be used for MgB_4O_7:Ce,Li films to allow for the decay of the prompt phosphorescence. A similar waiting time is recommended for Al_2O_3:C OSLDs [32].

3.3. *Other corrections needed*

As demonstrated and discussed in the previous Sections, MgB_4O_7:- Ce,Li requires no correction for pixel bleeding, but some phosphores- cence is still observed, probably due to retrapping of the charges at shallow traps associated with thermoluminescent peaks below room temperature. These can be corrected using the pixel-bleeding algorithm described by Yukihara and Ahmed [43], with the difference that, instead of the lifetime of 35 ms of the F-center in Al_2O_3, one would use the

ISSN: 2278-4632
Vol-10 Issue-2 No.01 February 2020

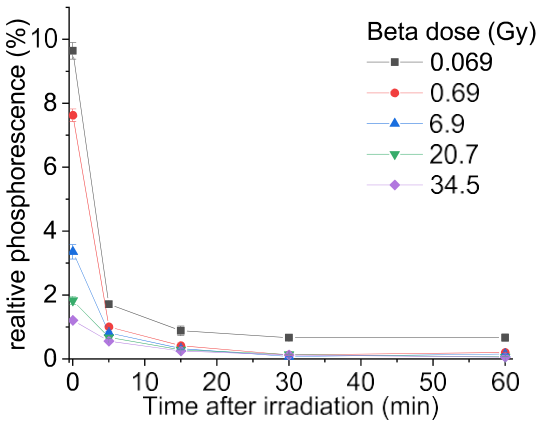

Fig. 6. Phosphorescence signal from five sets of three MgB_4O_7:Ce,Li samples immediately post irradiation with beta doses of 0.069 Gy–34.5 Gy relative to the initial OSL intensity.

MgB_4O_7:Ce,Li phosphorescence lifetimes determined for the specific setup. For the corrections, the lifetime was estimated using the 2D laser scanning system and the results obtained were 4.5 ms and 93 ms.

In the current 2D OSL reader prototype other system corrections are still necessary. Examples are the light collection efficiency correction and the geometrical distortion [43]. In this case, the same corrections applied by Ahmed et al. [44] were used, since these are not material dependent. To demonstrate these corrections in the case of the MgB_4O_7:Ce,Li films, Fig. 7 shows the image before and after the corrections. The image reconstruction algorithm was able to correct for the contribution due to phosphorescence signal in the raw image of the MgB_4O_7:Ce,Li film.

This data is, of course, just a demonstration, since the MgB_4O_7:Ce,Li films uniformity is not yet optimal and the exposure was not homoge- neous. Nevertheless, the objective is to show that the correction algo- rithm developed for Al_2O_3 films also works for MgB_4O_7:Ce,Li with small adjustments for the material characteristics. The phosphorescence correction required for MgB_4O_7:Ce,Li is much smaller than the pixel bleeding correction required for Al_2O_3 films. The parameter *R* [43], the

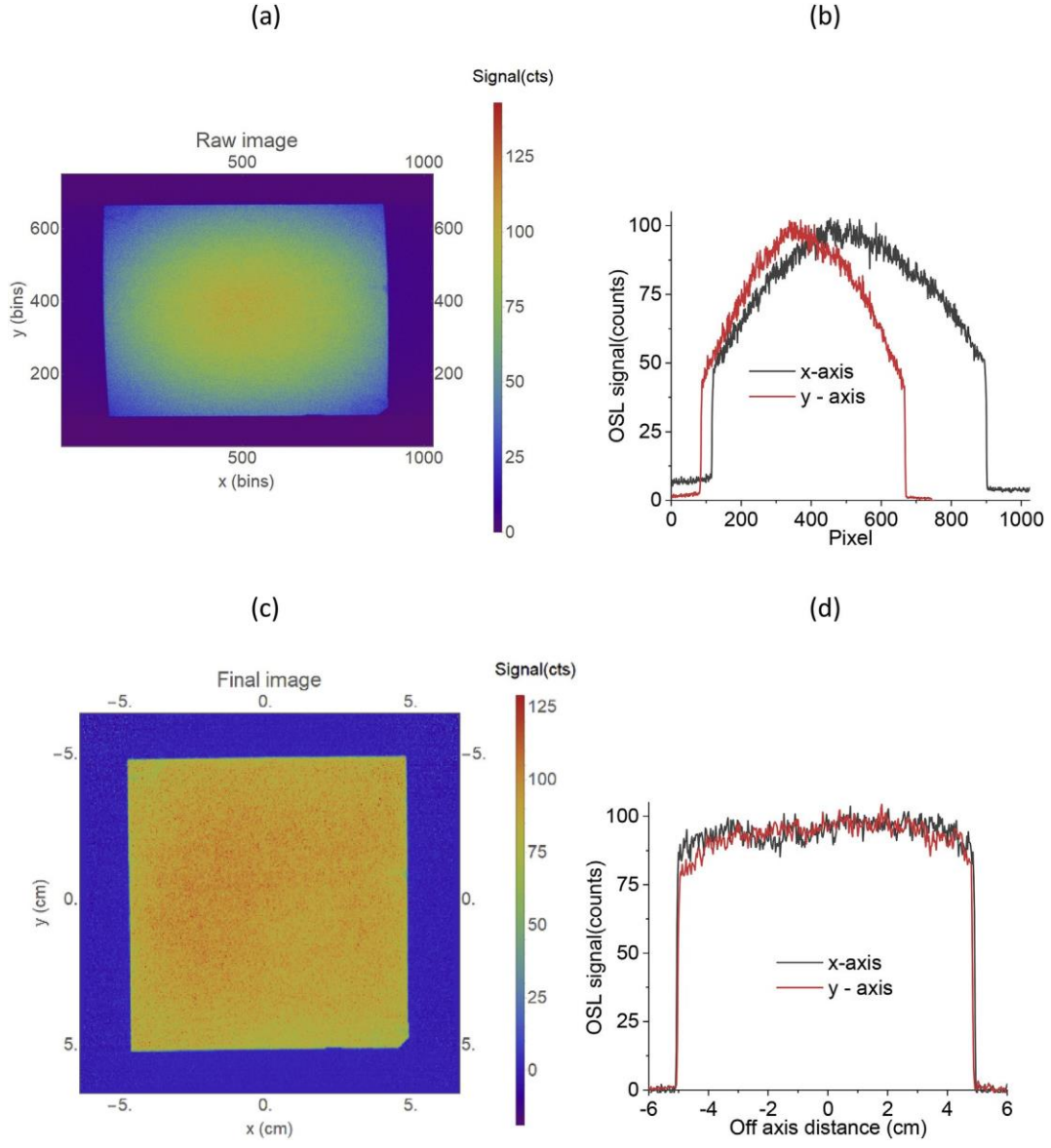

Fig. 7. (a) Raw image from the 10.0 cm × 10.0 cm MgB_4O_7:Ce,Li film irradiated using 90 kVp x-ray source in air with ~2.0 Gy total dose and (b) two signal profiles through the center of the image (average of 2 mm). (c) and (d) are similar data after image correction. The bin sizes in the raw images (a and b) are ~0.13 mm x ~0.17 mm in the x and y directions (see Sections 2.2.1 and 2.4), whereas the pixel size in the corrected images (c and d) are 0.25 mm × 0.25 mm.

ISSN: 2278-4632
Vol-10 Issue-2 No.01 February 2020

ratio between the slow components (phosphorescence and F-center emission in Al_2O_3) and the fast component, was found to be $R \sim 0.01–0.05$ for MgB_4O_7:Ce,Li compared to $R \sim 0.5$ and 0.35 for Al_2O_3:C and Al_2O_3:C,Mg films, respectively. Again, this demonstrates that the amount of pixel bleeding correction is minimized for MgB_4O_7:Ce, Li.

The laser scanning reader used here was developed for Al_2O_3:C and Al_2O_3:C,Mg and optimized for these materials, particularly regarding the choice of the scan speed. The scan speed or pixel dwell time could not be reduced below 327 µs because of the long luminescence lifetime of the F- centers in Al_2O_3 (35 ms) and the pixel bleeding correction [43,44]. In the case of MgB_4O_7:Ce,Li, however, this scan speed can be increased because of the fast Ce^{3+} luminescence lifetime (31.5 ns). This has also the advantage that faster scanning speeds lowers the contribution from phosphorescence components and reduces the need to correct for it.

To demonstrate that, five 3.0 cm × 3.0 cm MgB_4O_7:Ce,Li film pieces were irradiated with a total dose of ~ 55 Gy using the 90 kVp x-ray source and read out with pixel dwell times of 20 µs, 40 µs, 81 µs, 163 µs, and 327 µs. Fig. 8a shows the signal profiles (average of 2.0 mm at center) from the images obtained with different scan speeds. With faster scans the signal also becomes weaker, as less trapped charges are stimulated, which may become insufficient for dosimetry of lower doses. This can be compensated by increasing the laser power or decreasing the stimulation wavelength, or both. Multiple scans can also be performed, but then without gain in readout time.

Nevertheless, with faster scan times we also see a decrease in the relative contribution of phosphorescence. This can be seen in Fig. 8b, which shows the signal profiles normalized to the mean signal at the center over a ROI (1.0 cm × 1.0 cm).

3.4. *Dosimetric properties*

Even though the MgB_4O_7:Ce,Li films are not yet optimized,

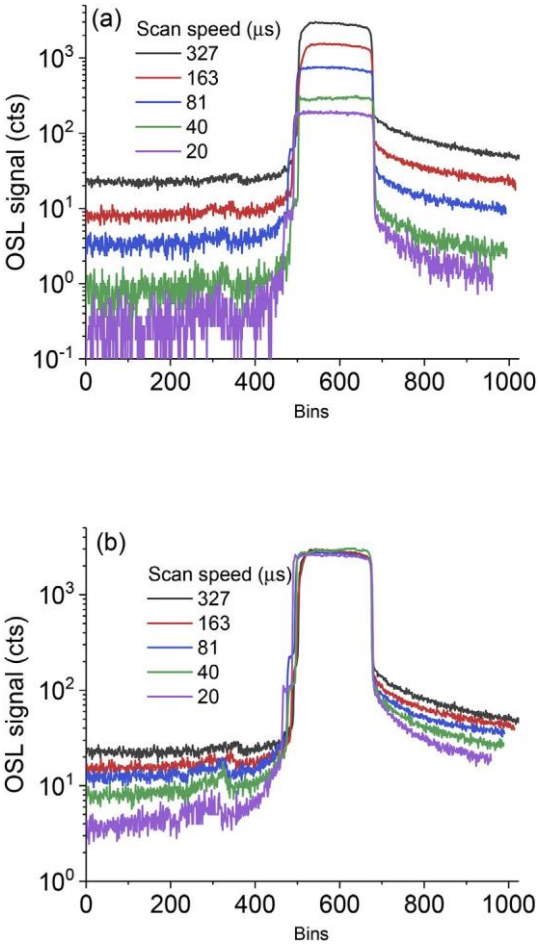

Fig. 8. (a) OSL signal profiles from 5 pieces of ~3.0 cm × 3.0 cm MgB_4O_7:Ce,Li film irradiated with a total dose of ~ 55 Gy scanned with pixel dwell times of 20 µs, 40 µs, 81 µs, 163 µs, and 327 µs Each signal profile is an average of a ~2.0- mm-wide film region. The signal profiles are from raw images before any correction. (b) OSL signal profiles from (a) normalized to the mean signal at the center over a ROI (1.0 cm × 1.0 cm).

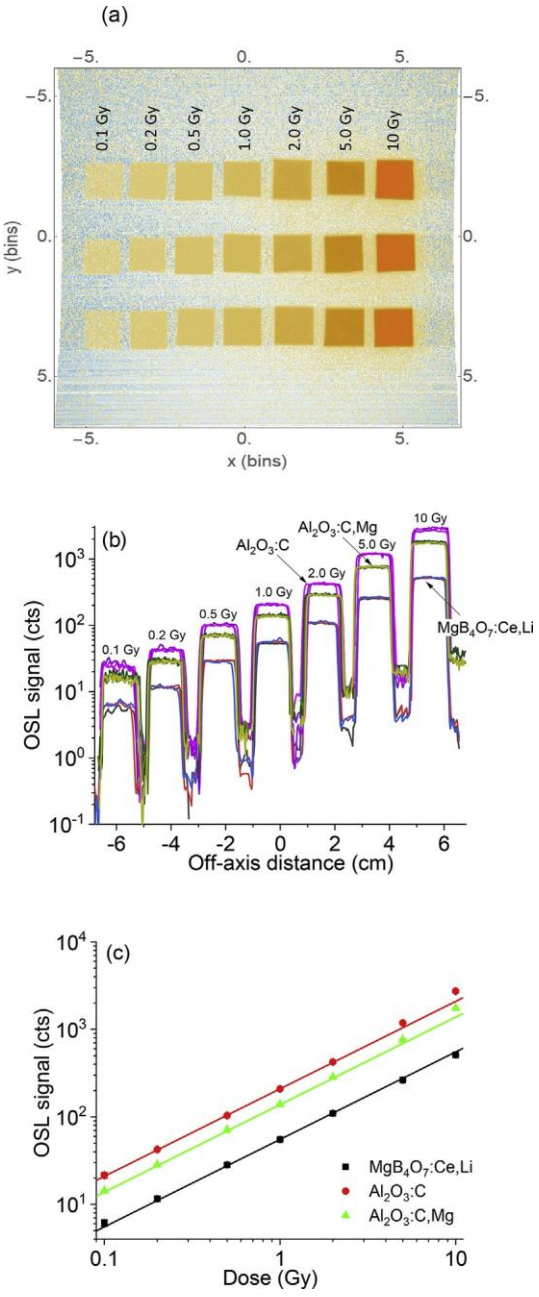

Fig. 9. (a) Image obtained from readout of three sets of small pieces of MgB_4O_7:Ce,Li detectors (~ 1.0 cm × 1.0 cm). Three samples were irradiated at each dose. (b) Signal profiles from the three detectors from each material type MgB_4O_7:Ce,Li, Al_2O_3:C and Al_2O_3:C,Mg in y-direction of the image. Each signal profiles is averaged over a width of ~ 2.0 mm from the center of the image. (c) Dose response curve of the MgB_4O_7:Ce,Li, Al_2O_3:C and Al_2O_3:C,Mg detectors. Each data point is an average signal calculated over 5.0 mm × 5.0 mm (~20 pixels × 20 pixels) around the central axis. The error bars in (c) represent the standard deviation of the mean based on the signal from three detectors.

ISSN: 2278-4632
Vol-10 Issue-2 No.01 February 2020

preliminary tests were performed to evaluate their dosimetric properties and identify potential problems.

3.4.1. Dose response

The dose response study was performed using 21 samples of MgB_4O_7:Ce,Li, Al_2O_3:C and Al_2O_3:C,Mg films each, of approximately 1.0 cm × 1.0 cm. The detectors were irradiated with doses ranging from 0.1 Gy to 10 Gy (100 mCi $^{90}Sr/^{90}Y$ beta source) using three detectors for each dose. The samples were read simultaneously two days after irradi- ation using the 2D reader. The objective here is not only to determine the dose response of the material, but also to test the dose response in con- ditions that simulated very steep dose gradients between the regions of the film with and without samples.

Fig. 9a shows the reconstructed image after all corrections for MgB_4O_7:Ce,Li detectors. Each column of detectors correspond to one dose, the doses increasing in the positive x-direction. The image shows a good separation between the detector pieces. The background signal around the samples increases with the dose, probably due to stimulation of the film by laser light scattered in the optical filters.

Fig. 9b shows signal profiles, averaged over a width of ~ 2.0 mm from the center of each row of dosimeters, for the three sets of detectors. Profiles based on Al_2O_3:C and Al_2O_3:C,Mg (images not shown) are also included for comparison. The image shows a good repeatability of the data.

Fig. 9c shows that the dose response of MgB_4O_7:Ce,Li is linear over the dose range investigated, whereas for the Al_2O_3 films supralinearity sets in. The figure shows the average signal of three detectors for each dose calculated over 5.0 mm × 5.0 mm (~20 pixels × 20 pixels) around the central axis. The error bars represent the standard deviation of the mean signal of three detectors. In fact, the dose response of MgB_4O_7 is reported to be linear until >10 Gy, becoming supralinear at higher doses with no saturation until 1000 Gy, whereas Al_2O_3:C departs from the linearity >1 Gy with saturation around 100 Gy [47]. The results from Fig. 9c confirm this finding. The lower sensitivity of these MgB_4O_7:Ce,Li films point to a lower material surface density as the cause, since the lower effective atomic number does not play a role in the beta irradia- tions. The sensitivity can still be optimized by increasing the film thickness or changing the readout parameters (increasing stimulation intensity or decreasing the stimulation wavelength, or both), but at the moment the sensitivity seems to be sufficient for 2D dosimetry in radiotherapy.

3.4.2. Re-usability of the films

In spite of the low signal depletion per readout reported in the Section 3.2.1, the OSL signal from MgB_4O_7:Ce,Li films could be bleached by optical stimulation using the bleaching unit described in Section 2.2.3. To demonstrate that, a 7.0 cm × 7.0 cm MgB_4O_7:Ce,Li film previously irradiated with dose of ~ 10 Gy was bleached overnight using the bleaching unit and read using the 2D OSL system (Section 2.2.1). At this point we just want to demonstrate that the signal can be bleached. The amount of time required for bleaching depends on the lamp spectrum and intensity; more detailed information can be found in Jursinic [54].

Fig. 10 shows the raw image of the bleached film (a) as well as the central dose profiles (b), where the dose was calculated using the cali- bration curve presented later in Section 3.4.1. Although the central part of the film is clearly visible (Fig. 10a), the average film background was only 0.02 counts bin^{-1}, which is equivalent to less than 0.5 mGy (Fig. 9c). This residual dose level is negligible compared to the typical doses used in radiation therapy.

3.4.3. Sensitization

The sensitization was determined using twelve MgB_4O_7:Ce,Li samples (7.0 mm diameter discs) irradiated repeatedly with beta dose of 0.69 Gy, 2.07 Gy, 6.9 Gy and 20.7 Gy. After each irradiation, the samples were read and bleached overnight using the bleaching unit (Section 2.2.3). This cycle was repeated for five runs.

Fig. 11 shows the initial OSL intensity and OSL area normalized to the first measurement for samples irradiated with repeated doses of 0.69 Gy, 2.07 Gy, 6.9 Gy and 20.7 Gy. The degree of sensitization is clearly dose-dependent, increasing with increasing doses. The average of the last 10 s of stimulation were used as background and subtracted from the signal.

It has been proposed that sensitization of the OSL signal in MgB_4O_7:Ce,Li is likely due to the incomplete bleaching of trapping cen- ters [48], but this has not yet been investigated in detail. Bleaching can be sufficient to reduce the OSL signal to background levels, but not necessarily to empty all trapping centers which can affect the sensitivity.

3.4.4. Fading

Fading of the MgB_4O_7:Ce,Li OSL films was determined by irradiating

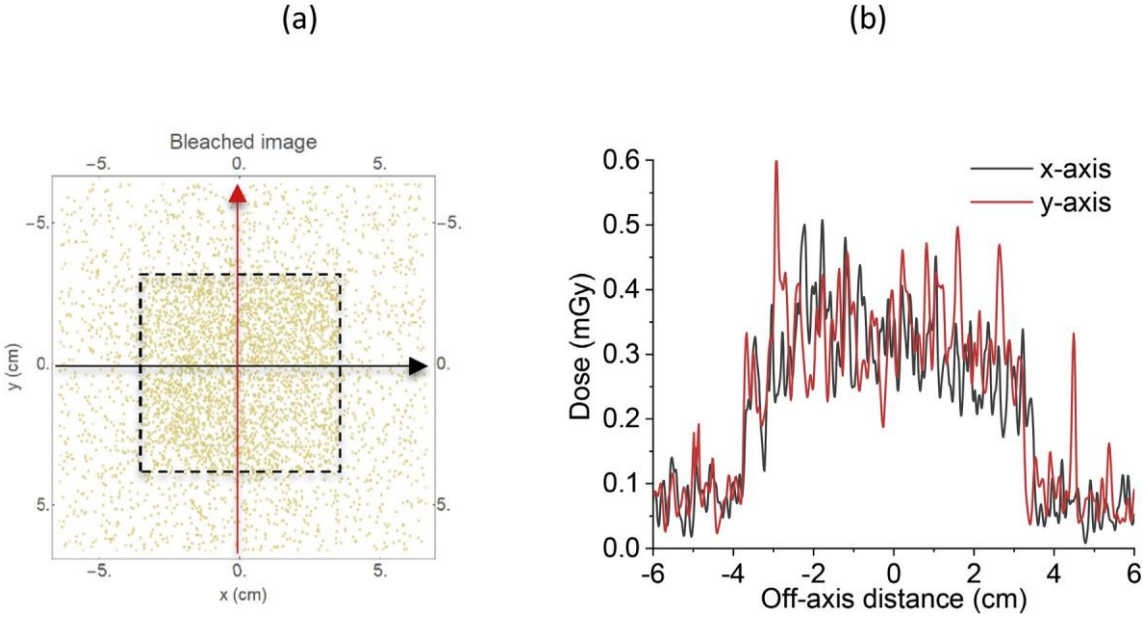

Fig. 10. (a) Raw OSL image from a bleached 7.0 cm × 7.0 cm MgB_4O_7:Ce,Li film previously irradiated with dose of ~ 10 Gy. The image was processed using 5 pixels × 5 pixels Wiener filter to reduce noise. (b) Signal profiles (average of all rows and columns) in both x and y direction from the MgB_4O_7:Ce,Li image in (a).

ISSN: 2278-4632
Vol-10 Issue-2 No.01 February 2020

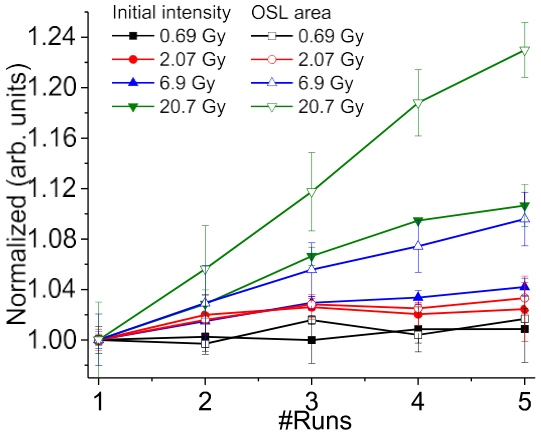

Fig. 11. OSL initial intensity and OSL area for repeated irradiation and bleaching normalized to run 1 for different doses. The error bars indicate the standard deviation of the 3 samples. After each run, the samples were bleached overnight using the bleaching unit (Section 2.2.3).

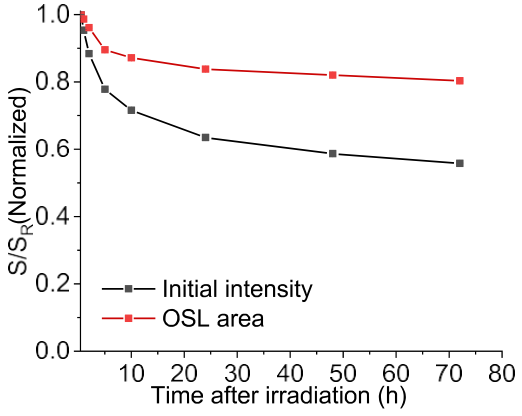

Fig. 12. OSL dark fading of MgB_4O_7:Ce,Li samples irradiated with 2.1 Gy. The signal is normalized to the OSL signal at 30 min after irradiation.

27 MgB_4O_7:Ce,Li samples (7.0 mm diameter disc) with ~2.1 Gy using the Risø beta source and storing them in the dark for various periods up to 72 h. After pre-defined periods, the OSL curve of three samples were read using the Risø reader (TL/OSL-DA-15) using green stimulation to record a signal *S*. After that, the samples were again irradiated with ~2.1 Gy and the signal was read immediately afterwards to record a reference signal S_R. The ratio S/S_R is the result normalized to the sample sensitivity and corrected for any possible system sensitivity variation. The S/S_R value was then normalized to the ratio for the samples read 30 min after irradiation.

Fig. 12 shows the MgB_4O_7:Ce,Li OSL fading for the initial intensity (average of first 3 s of stimulation) and total OSL area (total 600 s of stimulation). These results are similar to powder results obtained using a previous formulation based on low-purity reagents [47].

4. Conclusions and future developments

The results demonstrate the fast luminescence lifetime associated with Ce^{3+} emission (~31.5 ns) offers an advantage for 2D dosimetry for laser-scanning readout, minimizing the importance of pixel-bleeding correction. The OSL signal could be satisfactorily bleached using a bleaching unit consisting of fluorescence lamps and a long-pass filter. A
dose response curve could be obtained with pieces of films simulating steep dose gradients and the dose response obtained using the signal from the center of such piece films was linear up to 10 Gy. Short and long-term phosphorescence components were observed in the luminescence signal of MgB_4O_7:Ce,Li, but their contribution with respect to the fast OSL signal is relatively low and should decrease with the increase in the laser scan speed.

The main disadvantage of MgB_4O_7:Ce,Li at the moment is the lack of understanding of the processes responsible for the sensitivity changes and fading of the OSL signal. Although the bleaching unit used here allowed to reduce the residual OSL signal to minimum levels (<1 mGy), the sensitivity of the films increased with previous dose. Fading has also
been observed affecting the initial OSL intensity more than the OSL area. Therefore, the results demonstrate the potential of developing a convenient 2D dosimeter based on the OSL of MgB_4O_7:Ce,Li. Neverthe- less, future research should aim at identifying the causes for the sensi- tivity changes and fading, so that these problems can be minimized by the use of appropriate bleaching or pre-readout procedures, or by further material developments to reduce the trapping centers associated with these processes.

References

[1] E.E. Klein, J. Hanley, J. Bayouth, F.-F. Yin, W. Simon, S. Dresser, C. Serago, F. Aguirre, L. Ma, B. Arjomandy, C. Liu, C. Sandin, T. Holmes, Task Group 142 report: quality assurance of medical accelerators, Med. Phys. 36 (2009) 4197.
[2] J. Seco, B. Clasie, M. Partridge, Review on the characteristics of radiation detectors for dosimetry and imaging, Phys. Med. Biol. 59 (2014) R303–347.
[3] P. Montay-Gruel, K. Petersson, M. Jaccard, G. Boivin, J.F. Germond, B. Petit, R. Doenlen, V. Favaudon, F. Bochud, C. Bailat, J. Bourhis, M.C. Vozenin, Irradiation in a flash: unique sparing of memory in mice after whole brain irradiation with dose rates above 100Gy/s, Radiotherapy and oncology, J. Eur. Soc. Therapeut. Radiol. Oncol. 124 (2017) 365–369.
[4] M.C. Vozenin, J.H. Hendry, C.L. Limoli, Biological benefits of ultra-high dose rate FLASH radiotherapy: sleeping beauty awoken, Clin. Oncol. 31 (2019) 407–415.
[5] J. Bourhis, P. Montay-Gruel, P. Goncalves Jorge, C. Bailat, B. Petit, J. Ollivier, W. Jeanneret-Sozzi, M. Ozsahin, F. Bochud, R. Moeckli, J.F. Germond, M.C. Vozenin, Clinical translation of FLASH radiotherapy: why and how?, Radiotherapy and oncology, J. Eur. Soc. Therapeut. Radiol. Oncol. 139 (2019) 11–17.
[6] J. Bourhis, W.J. Sozzi, P.G. Jorge, O. Gaide, C. Bailat, F. Duclos, D. Patin, M. Ozsahin, F. Bochud, J.F. Germond, R. Moeckli, M.C. Vozenin, Treatment of a first patient with FLASH-radiotherapy, Radiotherapy and oncology, J. Eur. Soc. Therapeut. Radiol. Oncol. 139 (2019) 18–22.
[7] D.J. O'Brien, G.O. Sawakuchi, MRI-linac dosimetry: parameters that change in a magnetic field, Med. Phys. 43 (2016), 3874-3874.
[8] D.J. O'Brien, N. Schupp, S. Pencea, J. Dolan, G.O. Sawakuchi, Dosimetry in the presence of strong magnetic fields, J. Phys. Conf. Ser. 847 (2017).
[9] D.J. O'Brien, J. Dolan, S. Pencea, N. Schupp, G.O. Sawakuchi, Relative dosimetry with an MR-linac: response of ion chambers, diamond, and diode detectors for off- axis, depth dose, and output factor measurements, Med. Phys. 45 (2018) 884–897.A.J. Raaijmakers, B.W. Raaymakers, J.J. Lagendijk, Magnetic-field-induced dose effects in MR-guided radiotherapy systems: dependence on the magnetic field strength, Phys. Med. Biol. 53 (2008) 909–923.
[10] J.J.W. Lagendijk, M. van Vulpen, B.W. Raaymakers, The development of the MRI linac system for online MRI-guided radiotherapy: a clinical update, J. Intern. Med. 280 (2016) 203–208.
[11] A. Niroomand-Rad, C.R. Blackwell, B.M. Coursey, K. Gall, P.J.M. Galvin, W.L. McLaughlin, A.S. Meigooni, R. Nath, J.E. Rodgers, C.G. Soares, Radiochromic film dosimetry: recommendations of AAPM radiation therapy committee task group 55, Med. Phys. 25 (1998) 2093–2115.
[12] T.S. Stelljes, A. Harmeyer, J. Reuter, H.K. Looe, N. Chofor, D. Harder, B. Poppe, Dosimetric characteristics of the novel 2D ionization chamber array OCTAVIUS Detector 1500, Med. Phys. 42 (2015) 1528–1537.
[13] D. Letourneau, M. Gulam, D. Yan, M. Oldham, J.W. Wong, Evaluation of a 2D diode array for IMRT quality assurance, Radiother. Oncol. 70 (2004) 199–206.
[14] C.S. Porumb, A.H. Aldosari, I. Fuduli, D. Cutajar, M. Newall, P. Metcalfe, M. Carolan, M.L.F. Lerch, V.L. Perevertaylo, A.B. Rosenfeld, M. Petasecca, Characterisation of silicon diode arrays for dosimetry in external beam radiation therapy, IEEE Trans. Nucl. Sci. 63 (2016) 1808–1817.
[15] M. Tamponi, R. Bona, A. Poggiu, P. Marini, A new form of the calibration curve in radiochromic dosimetry. Properties and results, Med. Phys. 43 (2016) 4435–4446.
[16] M.P. Grams, J.M. Gustafson, K.M. Long, L.E. Fong de los Santos, Technical note: initial characterization of the new EBT-XD gafchromic film, Med. Phys. 42 (2015) 5782–5786.
[17] A. Micke, D.F. Lewis, X. Yu, Multichannel film dosimetry with nonuniformity correction, Med. Phys. 38 (2011) 2523.
[18] L. Lin, M. Kang, T.D. Solberg, T. Mertens, C. Baeumer, C.G. Ainsley, J.E. McDonough, Use of a novel two-dimensional ionization chamber array for pencil beam scanning proton therapy beam quality assurance, J. Appl. Clin. Med. Phys. 16 (2015).
[19] D.A. Low, J.M. Moran, J.F. Dempsey, L. Dong, M. Oldham, Dosimetry tools and techniques for IMRT, Med. Phys. 38 (2011) 1313–1338.
[20] B. Delfs, A.A. Schoenfeld, D. Poppinga, R. Kapsch, P. Jiang, D. Harder, B. Poppe, H.K. Looe, Magnetic fields are causing small, but significant changes of the radiochromic EBT3 film response to 6 MV photons, Phys. Med. Biol. 63 (2018), 035028.
[21] F.J. Reynoso, A. Curcuru, O. Green, S. Mutic, I.J. Das, L. Santanam, Technical note: magnetic field effects on gafchromic-film response in MR-IGRT, Med. Phys. 43 (2016) 6552–6556.
[22] M. Reynolds, B.G. Fallone, S. Rathee, Dose response of selected solid state detectors in applied homogeneous transverse and longitudinal magnetic fields, Med. Phys. 41 (2014) 12.
[23] M.F. Ahmed, N. Shrestha, E. Schnell, S. Ahmad, M.S. Akselrod, E.G. Yukihara, Characterization of Al_2O_3 optically stimulated luminescence films for 2D dosimetry using a 6 MV photon beam, Phys. Med. Biol. 61 (2016) 7551–7570.
[24] A. Jahn, M. Sommer, J. Henniger, 2D-OSL-dosimetry using beryllium oxide, Radiat. Meas. 45 (2010) 674–676.
[25] R. De Roover, C. Berghen, G. De Meerleer, T. Depuydt, W. Crijns, Extended field radiotherapy measurements in a single shot using a BaFBr-based OSL-film, Phys. Med. Biol. 64 (2019).
[26] Z.H. Han, J.P. Driewer, Y.S. Zheng, D.A. Low, H.H. Li, Quantitative megavoltage radiation

ISSN: 2278-4632
Vol-10 Issue-2 No.01 February 2020

therapy dosimetry using the storage phosphor KCl:Eu^{2+}, Med. Phys. 36 (2009) 3748–3757.
[27] J.J. Schuyt, G.V.M. Williams, Development of a 2D dosimeter using the optically stimulated luminescence of $NaMgF_3$:Eu with CCD camera readout, Radiat. Meas. 121 (2019) 99–102.
[28] W. Crijns, D. Vandenbroucke, P. Leblans, T. Depuydt, A reusable OSL-film for 2D radiotherapy dosimetry, Phys. Med. Biol. 62 (2017) 8441–8454.
[29] L. Bøtter-Jensen, S.W.S. McKeever, A.G. Wintle, Optically Stimulated Luminescence Dosimetry, Elsevier, Amsterdam, 2003.
[30] E.G. Yukihara, S.W.S. McKeever, Optically Stimulated Luminescence: Fundamentals and Applications, John Wiley & Sons, Chichester, West Sussex, UK, 2011.
[31] S.F. Kry, P. Alvarez, J.E. Cygler, L.A. DeWerd, R.M. Howell, S. Meeks, J. O'Daniel, C. Reft, G. Sawakuchi, E.G. Yukihara, D. Mihailidis, AAPM TG 191 clinical use of luminescent dosimeters: TLDs and OSLDs, Med. Phys. 47 (2020) e19–e51.
[32] C.K. Spindeldreier, O. Schrenk, M.F. Ahmed, N. Shrestha, C.P. Karger, S. Greilich, A. Pfaffenberger, E.G. Yukihara, Feasibility of dosimetry with optically stimulated luminescence detectors in magnetic fields, Radiat. Meas. 106 (2017) 346–351.
[33] P. Leblans, D. Vandenbroucke, P. Willems, Storage phosphors for medical imaging, Materials 4 (2011) 1034–1086.
[34] J.A. Rowlands, The physics of computed radiography, Phys. Med. Biol. 47 (2002) R123–R166.
[35] H.H. Li, A.L. Gonzalez, H. Ji, D.M. Duggan, Dose response of BaFBrI:Eu^{2+} storage phosphor plates exposed to megavoltage photon beams, Med. Phys. 34 (2007) 103–111.
[36] E. Ariga, S. Ito, S. Deji, T. Saze, K. Nishizawa, Development of dosimetry using detectors of diagnostic digital radiography systems, Med. Phys. 34 (2007) 166–174.
[37] A.J. Olch, Evaluation of a computed radiography system for megavoltage photon beam dosimetry, Med. Phys. 32 (2005) 2987–2999.
[38] H.L. Liu, R.J.R. Liu, D.M. Reeve, S.J. Shepard, C.E. Willis, Measurement of CT radiation profile width using CR imaging plates, Med. Phys. 32 (2005) 2881–2887.
[39] K. Idri, L. Santoro, E. Charpiot, J. Herault, A. Costa, N. Ailleres, R. Delard, J.R. Vaille, J. Fesquet, L. Dusseau, Quality control of intensity modulated radiation therapy with optically stimulated luminescent films, IEEE Trans. Nucl. Sci. 51 (2004) 3638–3641.
[40] H.H. Li, J.P. Driewer, Z. Han, D.A. Low, D. Yang, Z. Xiao, Two-dimensional high spatial-resolution dosimeter using europium doped potassium chloride: a feasibility study, Phys. Med. Biol. 59 (2014) 1899–1909.
[41] M.F. Ahmed, S. Eller, E. Schnell, S. Ahmad, M.S. Akselrod, E.G. Yukihara, Development of a 2D dosimetry system based on the optically stimulated luminescence of Al_2O_3, Radiat. Meas. 71 (2014) 187–192.
[42] E.G. Yukihara, M.F. Ahmed, Pixel bleeding correction in laser scanning luminescence imaging demonstrated using optically stimulated luminescence, IEEE Trans. Med. Imag. 34 (2015) 2506–2517.
[43] M.F. Ahmed, E. Schnell, S. Ahmad, E.G. Yukihara, Image reconstruction algorithm for optically stimulated luminescence 2D dosimetry using laser-scanned Al_2O_3 films, Phys. Med. Biol. 61 (2016) 7484–7506.
[44] H. von Seggern, Photostimulable X-ray storage phosphors: a review of present understanding, Braz. J. Phys. 29 (1999) 254–268.
[45] M.F. Ahmed, N. Shrestha, S. Ahmad, E. Schnell, M.S. Akselrod, E.G. Yukihara, Demonstration of 2D dosimetry using Al_2O_3 optically stimulated luminescence films for therapeutic megavoltage x-ray and ion beams, Radiat. Meas. 106 (2017) 315–320.
[46] E.G. Yukihara, B.A. Doull, T. Gustafson, L.C. Oliveira, K. Kurt, E.D. Milliken, Optically stimulated luminescence of MgB_4O_7:Ce,Li for gamma and neutron dosimetry, J. Lumin. 183 (2017) 525–532.
[47] T.D. Gustafson, E.D. Milliken, L.G. Jacobsohn, E.G. Yukihara, Progress and challenges towards the development of a new optically stimulated luminescence (OSL) material based on MgB_4O_7:Ce,Li, J. Lumin. 212 (2019) 242–249.
[48] L.F. Souza, A.M.B. Silva, P.L. Antonio, L.V.E. Caldas, S.O. Souza, F. d'Errico, D.N. Souza, Dosimetric properties of MgB_4O_7:Dy,Li and MgB_4O_7:Ce,Li for optically stimulated luminescence applications, Radiat. Meas. 106 (2017) 196–199.
[49] T. Lapp, M. Kook, A.S. Murray, K.J. Thomsen, J.-P. Buylaert, M. Jain, A new luminescence detection and stimulation head for the Risø TL/OSL reader, Radiat. Meas. 81 (2015) 178–184.
[50] T. Lapp, M. Jain, C. Ankjaergaard, L. Pirtzel, Development of pulsed stimulation and Photon Timer attachments to the Risø TL/OSL reader, Radiat. Meas. 44 (2009).
[51] N.K. Umisedo, E.M. Yoshimura, P.B.R. Gasparian, E.G. Yukihara, Comparison between blue and green stimulated luminescence of Al_2O_3:C, Radiat. Meas. 45 (2010) 151–156.
[52] G. Denis, M.G. Rodriguez, M.S. Akselrod, T.H. Underwood, E.G. Yukihara, Time- resolved measurements of optically stimulated luminescence of Al_2O_3:C and Al_2O_3: C,Mg, Radiat. Meas. 46 (2011) 1457–1461.
[53] P.A. Jursinic, Characterization of optically stimulated luminescent dosimeters, OSLDs, for clinical dosimetric measurements, Med. Phys. 34 (2007) 4594–4604.